PREDICTION OF LAMINAR/TURBULENT TRANSITION IN AN UNSTRUCTURED FINITE ELEMENT NAVIER STOKES SOLVER USING A BOUNDARY LAYER CODE WITH EMPHASIS ON CROSS FLOW TRANSITION

50th 3AF INTERNATIONAL CONFERENCE ON APPLIED AERODYNAMICS
Toulouse, France, 29-30 March - 01 April 2015

Raphael Gross [(1)], Jean-Claude Courty [(2)],
Dac Tran [(3)], Michel Mallet [(4)]
Daniel Arnal [(5)], Olivier Vermeersch [(6)], David Hue [(7)]

[(1)] *Raphe_g@hotmail.com*, [(2)] *jc.courty2a@gmail.com*
[(3)] [(4)] *Dassault Aviation, 78, **quai** Marcel Dassault 92552 Saint-Cloud FRANCE, Dac.Tran@Dassault-Aviation.com, Michel.Mallet@Dassault-Aviation.com*
[(5)] [(6)] *ONERA, 2 Avenue Édouard Belin, 31000 Toulouse FRANCE, Daniel.Arnal@ONERA.fr, Olivier.Vermeersch@ONERA.fr, David.Hue@ONERA.fr*

1. ABSTRACT

This paper presents some developments performed to achieve an accurate and efficient prediction tool for laminar/turbulent transition. These developments involve industrial codes used at Dassault Aviation for the aerodynamics design of military aircraft and business jets. The process is based on a flexible sequence of simulation tools. The issues concerning influence of the numerical solvers, transition onset criteria and the coupling process are described. The influence of intermittency function is also discussed. Results demonstrate the accuracy of the method with emphasis on transition induced by crossflow instabilities.

Key Words: *unstructured RANS solver, transition criteria, Database method, e^N method, boundary layer code.*

2. NOMENCLATURE

δ_e = *boundary layer thickness*
γ = *intermittency function*
$\cdot_e$ = *taken at the boundary layer edge*
$\cdot_a$ = *local wing coordinate system*
s = *curvilinear abscissa*
C = *chord*
$N_{CF_{limit}}$ = *N triggering CF induced transition.*
$N_{CF_{Trans}}$ = fixed value *of* $N_{CF_{limit}}$ based on previous empirical value *(confidentially restriction).*
$N|NCF$ = *$N/N_{CF_{Trans}}$ (confidentially restriction).*
$(\vec{X},\vec{Y},\vec{Z})$ = *cartesian coordinate system with $\vec{X}$ the free stream direction and $\vec{Y}$ the cross direction.*
(U, V, W) = velocity field with respect to $(\vec{X},\vec{Y},\vec{Z})$
Abbreviations:
BL *Boundary Layer*
CF *Crossflow*
TS *Tollmien - Schlichting*

3. INTRODUCTION

With rising fuel costs and environmental requirements getting stricter, aircraft manufacturers are investigating the potential of new technologies in aircraft design. The prediction of transition from laminar to turbulent flow is still a major challenge. Various approaches [1] [2] are explored and new developments performed to improve both accuracy and facility of use of transition prediction.
Laminar airfoils would allow a theoretical 15% reduction in total aircraft drag. Design and optimization of such configurations, through computational fluid dynamics (CFD), and numerical and physical models for laminar to turbulent transition prediction are of importance. Reynolds Averaged Navier Stokes (RANS) simulations have reached a mature and validated capacity; they are used routinely for aerodynamic design.
In the first part of this paper, the process for transition prediction will be presented. It is based on a flexible sequence of simulation tools. The possible choices for each module will also be discussed, including the influence of the numerical solvers, transition definition criteria and the coupling process. This automated process can operate with multiple lifting surfaces: wing, horizontal stabilizer, slat and flaps. Furthermore, the process is fully compatible with the industrial unstructured 3D RANS code used for aircraft design.

4. DEVELOPMENT AND IMPLEMENTATION OF AUTOMATIC PREDICTION OF LAMINAR TURBULENT TRANSITION

The transition prediction numerical process has been developed by Dassault Aviation. This process relies on the in-house Navier Stokes (NS) solver Aether [3] coupled with the boundary layer

(BL) code 3C3D [4] from ONERA. This coupling significantly reduces computational costs, as the BL code reevaluates the BL velocity profiles by solving the simplified parabolic BL equations. Therefore fewer nodes in the near-wall region are needed when computing the RANS solution. The overall structure of the prediction process is described in Fig.1:

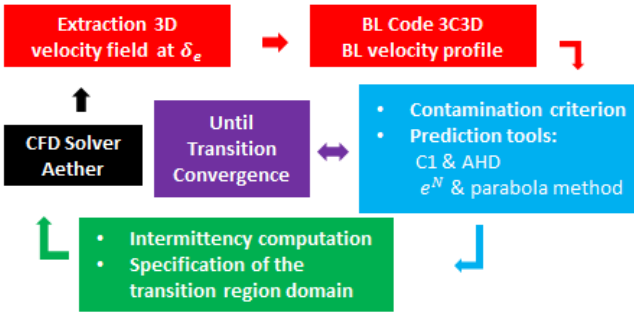


Figure 1: Transition prediction chain. Coupling structure between the RANS solver Aether and the boundary layer code 3C3D.

The present approach relies on the 3D velocity field at the BL edge provided by the NS solver to 3C3D in order to perform the boundary layer computations. This represents an improvement compared to alternative methods (e.g. [1] [2]) which use the pressure coefficient distribution with 2D, quasi-3D or conical hypothesis. Further assumptions on the nature of the transverse flow used by the latter yield slightly less accurate modeling of the CF instabilities (see §5.1).

4.1. Numerical solvers

Aether is an unstructured three dimensional, compressible Navier-Stokes solver. It allows tetrahedral and prismatic elements. The code is based on a finite element method using a streamline upwind Petrov-Galerkin stabilization scheme. The NS equations are symmetrized using entropy variables, thus yielding better mathematical properties for efficient preconditioning. Aether is fully parallelized and a large range of turbulence models is available, even though this study is restricted to the k-ε model with a wall-resolved modeling of the turbulent boundary layer.

3C3D is a three dimensional, compressible BL code. The BL equations are resolved with a finite difference method which is based on a characteristic method along external streamlines. Several turbulence models as well as transition criteria are available in 3C3D.

4.2. Communication between Aether and 3C3D:

In order to compute the BL velocity profiles with 3C3D, a projection of Aether's velocity field taken at the BL edge δ_e is made on a new structured mesh based on 3 plan cuts as represented in Fig.2 (a). To accelerate this process, the transition analysis is made for localized and limited number of sections (see Fig. 2(b)) of lifting surfaces (aircraft wing, horizontal tail plane, vertical fin, winglet, etc.); linear interpolation is used between them to determine the transition lines.

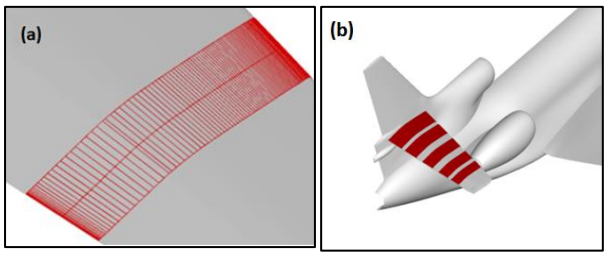


Figure 2: structured meshes used for 3C3D.
(a) Extraction process is made along cuts of the horizontal tail plane and the velocity field at δ_e is projected onto a new structured surface mesh used by 3C3D.
(b) The process is repeated for a defined number of sections.

4.3. Transition criteria

4.3.1. Contamination from the leading-edge

The contamination at the attachment line is caused by the junction between the fuselage and the wing. The transport of fuselage turbulence along the attachment line of the wing is enhanced by increased sweep angle and nose radius.

Therefore, it is necessary to determine whether or not the transition mechanism is caused by contamination. The attachment line contamination criterion [5] is characterized by the parameter:

$$\overline{R} = \frac{V_{a_e}}{\nu}\left[\frac{\nu}{\frac{dU_{a_e}}{ds}_{|s=0}}\right]^{0.5}$$

With V_{a_e} the transverse velocity value at δ_e (with respect to the attachment line), U_{a_e} the longitudinal velocity value at δ_e (with respect to the leading edge normal) and ν the viscosity. When $\overline{R}$>250, contamination occurs and the whole wing surface becomes turbulent. Whereas when $\overline{R}$<250, there is no contamination and the transition is predicted by the instability mechanism described in the following paragraph.

4.3.2. Instability mechanism

In free-flight conditions (low external turbulence and noise levels, good surface quality) the transition is said to be natural. External disturbances or small average surface roughness will activate a phenomenon called receptivity.

Receptivity describes the process through which instabilities are created in the BL.
Instabilities are characterized by their frequencies, wavelengths and the corresponding spatial growth rates. Two kinds of disturbances may lead to the natural transition: the Tollmien-Schlichting [6] (noted TS) waves linked to the longitudinal velocity profile and amplified by a positive pressure gradient or the cross flow [7] (CF) instabilities generated by the transverse velocity profile occurring with the adverse pressure gradient (e.g. close to the leading edge). These disturbances are amplified in the streamwise direction until one reaches critical amplitude thus triggering the transition to turbulence.

4.3.3. Semi-empirical criteria

The natural transition is determined by using semi-empirical criteria based on BL integral parameters (Mach number M_e, incompressible shape factor H_i, etc.). For instance, AHD [7] criterion for TS induced transition and the C1 [7] criterion for CF induced transition have been developed at ONERA. The first criterion that reaches its limit value defines the transition location.
AHD criterion takes the BL stability history into account through the mean Pohlhausen parameter.
Nonetheless, C1 criterion is derived from experimental data and explanatory variables used are local ones (δ_2, H_i, M_e, R_e). Therefore, it doesn't take into account flow stability history and can display in some cases discrepancies with respect to experimental data.

4.3.4. Linear stability

A more sophisticate approach to compute the transition lies in the Linear Stability theory [8].
A local wing coordinate system is defined with $\vec{X}_a$ as the perpendicular direction to the leading edge, $\overrightarrow{Y_a}$ as the spanwise direction and $\vec{Z}_a$ the normal to the wall.
The velocity field of the mean flow is (U_a, V_a, W_a) in the local coordinate system $(\vec{X}_a, \vec{Y}_a, \vec{Z}_a)$.
In the framework of local stability theory, the BL flow is supposed to be locally parallel. The linear growth of small disturbances added to the base flow in context of spatial theory is described by eq.1:

$$q(x,y,z,t) = q'(z).\exp(-\alpha_i x)\exp\big(i(\alpha_r x + \beta y - \omega t)\big) \quad \text{eq.1}$$

- q is any fluctuating quantity;
- $\omega = \frac{2\pi f \delta_1}{U_e}$ is the dimensionless circular frequency;
- The real part (α_r, β) of the wave number defines the wave vector, hence the parameter $\Psi(\beta, \alpha_r)$:

$$\Psi = \tan^{-1}\frac{\beta}{\alpha_r} - \vartheta$$

Where ϑ is the angle between $\vec{X}_a$ and $\vec{X}_e$ (the tangent to the external streamline).

- α is a complex number. $-\alpha_i$>0 (respectively $-\alpha_i$<0) corresponds to the amplification (respectively to the damping) of the disturbance.
  The growth rate for a given frequency is determined by the $N(f)$ factor between x_0 (the abscissa where $-\alpha_i = 0$ and x (the position of interest) :

$$N(f) = \int_{x_0}^{x} \max_{\Psi} -\alpha_i(f)\, dx$$

  The envelope N factor is obtained by taking the largest amplification rate for a broad range of frequencies *f.*

Parameters N and Ψ can be evaluated by two methods:

- Exact linear Stability using the code CASTET [9]. By substituting eq.1 in the NS equation and using the linear stability assumption made before we obtained the Orr-Sommerfeld equation. The no slip boundary condition at the wall as well as the fact that the perturbation must vanish far from the BL provide an eigenvalue problem. This problem has non trivial sets of solution. Therefore, a shooting method is used starting from initial conditions.
- The Parabola method [10] is based on a database of exact linear stability results of the Falkner and Skan velocity profiles. The inputs include velocity and temperature profiles, and BL integral values. This tool has the advantage of being fully automated. In other words, it does not need initial values. Due to the pre-existent linear stability database results, almost no computation is to be made. This implies a huge gain in time with regards to a stability solver.

4.3.5. e^N criterion :

The acquired experience from analyses of empirical results of wind tunnel and flight data between ONERA, Dassault Aviation and their partners' allows us to establish the current transition strategy criterion:

- If the flow is 2D, the transition is achieved when the N factor reaches its limited value N_{limit} determined by the Mack law [11], function of the turbulent rate Tu.

$$N_{limit} = N_{TS_{limit}} = N_{Mack}$$
$$N_{Mack} = -8.43 - 2.4ln(Tu)$$

- If the flow is 3D, two configurations occur: At the leading edge, CF instabilities are amplified due to the high transverse velocity

value. TS instabilities are damped due to the negative pressure coefficient. The flow is said to be CF dominated (Ψ>60°). If the N factor is higher than $N_{CF_{limit}} = N_{CF_{Trans}}$, the transition is triggered. Otherwise, the transition is triggered further downstream by TS instabilities when the N factor reaches the limit:
$N_{limit} = N_{CF_{max}} + N_{TS_{limit}}$ where $N_{CF_{max}}$ denotes the maximum of N in the CF dominated zone (Ψ>60°) and $N_{TS_{limit}}$ is obtained by the Mack formula as with 2D flow.

Note:

- $N_{CF_{Trans}}$ is a fixed value based on previous empirical value.
- If there are more than 2 zones (i.e. alternating sequence of CF/TS) the transition criterion is no longer valid. This will be illustrated in the last part, regarding the horizontal tail plane of the Falcon 7X for Y=0.74 (section 2).
- Ψ parameter can show some local discontinuities for the parabola method. In order to have an automatized process for transition prediction, smoothing is needed. Thus, a shifting between CF and TS is identified when the new CF or TS zone happens to be greater than 5% of chord.

4.4. Intermittency function:

The preliminary computations have shown a discontinuity in the pressure coefficient distribution corresponding to transition location. This numerical artifact was due to the sharp transition between laminar and turbulent flows and could prevent the convergence of the transition position during coupling. This has been overcome using an intermittency function noted γ (ex: Arnal & Coustols [12], etc.) as a factor of the effective viscosity term μ. The intermittency function has multiple advantages: it averages out the numerical artifact, improves the convergence of the computation and better matches the physics itself.

4.5. Coupling process

At each given number of iterations of Aether process to resolve the RANS equations, the transition lines of the lifting surface selected by the user are evaluated and communicated to Aether through the γ variable computed over the entire computational domain. This coupling process is repeated until each transition line converges. In order to accelerate the convergence of the transition, under-relaxation is used and sonic shock detection is carried out. If transition is detected near the shock location, there is no use of intermittency function. This is essential to secure residual convergence. When transition is triggered at the foot of the shock, the RANS computation can become unsteady due to boundary flow separation.

5. METHODOLOGY & VALIDATION

Due to confidentially restriction the spanwise parameter Y is non-dimensional and N factor is substituted by $N|NCF = N/N_{CF_{Trans}}$.

In the present framework, transition chain methodologies and hypotheses are first analyzed and compared to results obtained with ONERA solver (Elsa). The case used in this section is the Low Speed Business Jet (LSBJ) case defined in the framework of Clean Sky/SFWA project dedicated to the study of innovative aerodynamics devices. *In addition, this configuration will be tested at the ETW wind tunnel in 2015.* ***No optimization for laminarity was performed*** **on pressure side, only for the suction side.**

The Mach number is 0.8 and the Reynolds number is 4.5 million/m.

Since $\bar{R}$ is less than 250 (Fig. 3), the transition prediction analysis on the wing can be carried out.

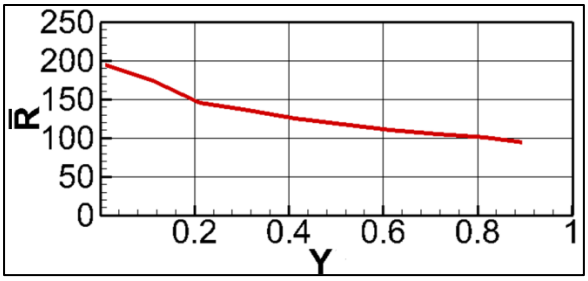


Figure 3: spanwise evolution of $\bar{R}$*, LSBJ configuration. No contamination detected (*$\bar{R}$ *<250)*

5.1. Comparison between 2.5D assumption, local 3D and 3D.

The innovative part in the process described in §4.2 is the use of Aether (NS solver) 3D velocity field at δ_e as 3C3D (the BL code) input. Generally, the transverse velocity component V_e is assumed constant (2.5D assumption) along streamwise direction with respect to the effective sweep angle φ_{eff} ($V_e = U_\infty \sin \varphi_{eff}$).

There are mostly three practical reasons to use 2.5D assumption. These reasons are discussed below in order to promote the 3D local method used in Dassault Aviation transition chain:

3C3D BL computation	2.5D	Local 3D (Fig. 2)	FULL WING 3D computation
New structured mesh generation	NO	mesh based on 3 plan cuts	YES
δ_e	NO	YES	YES
V_e	$V_e = U_\infty \sin$	V_e	V_e
U_e	$U_e = f(P_w)$	U_e	U_e

With 2.5D assumption there is no need to generate

a structured surface mesh and to project the velocity field at δ_e on it. Moreover compared to 3D method, it is time saving when many transition analyses are to be made (ex: optimization of a wing needs thousands of iterations involving thousands of different meshes).
Doing slices over the wing and constructing local structured meshes overcome the difficulties of generating new meshes over the complete wing. Even for complex geometries, it is trivial and the cost is negligible. The tasks are parallelizable compared to a full 3D BL computation over the whole wing.
With 2.5D method, the pressure at the wall can be taken to conduct the BL computation with the BL code which spares the evaluation of the velocity at δ_e. However this assumption is based on the fact that pressure is constant along the BL thickness which is in practice not true, there is a slight difference.
2.5D or conical assumption gives good results and may be sufficient in most cases but for real 3D flow or when leading/trailing edges sweep angles are too different, a significant error is noticed while 3D methods yield perfect match.
Fig.4 displays a comparison between N factor evaluated with the parabola method for 2.5D assumption (green), local 3D analysis (blue) and the 3D analysis (made with a structured mesh over the entire wing) (red). This plane cut is made at 5% after the beginning of the wing, near the Karman (which is subject to an optimization process at Dassault Aviation in order to delay the transition in this region).

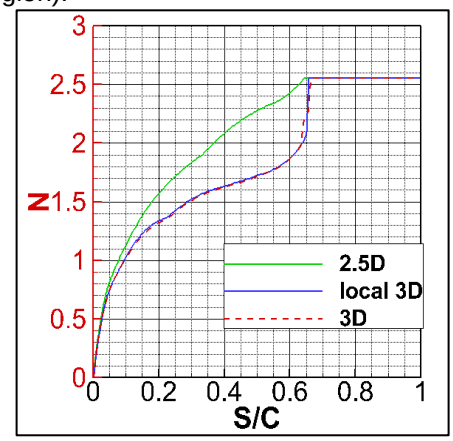


Figure 4: LSBJ test case, section Y=5%. Evolution of the N factor evaluated with 3C3D velocity field and using the parabola method.

Results are in agreement along the 3 methods for the leading edge. Further downstream, differences between 2.5D and 3D methods are more apparent whereas 3D methods (local 3D and fully 3D) are superposed.
Fig.5 demonstrates the effect of transverse velocity assumption. The velocity profiles obtained with 3C3D are displayed for 3 stations. The first one is extracted at 10% chord (red line 2.5D method, red dotted line for 3D) from the leading edge, the second at 20% (green lines) and the third at 55% (blue lines). The constant sweep angle used along x tends to overestimate the transverse velocity profiles. For S/C= 0.1 the error is small but for S/C=0.55 the inflexion point location and velocity, which are two essential parameters used to compute the N factor, are totally miscalculated.

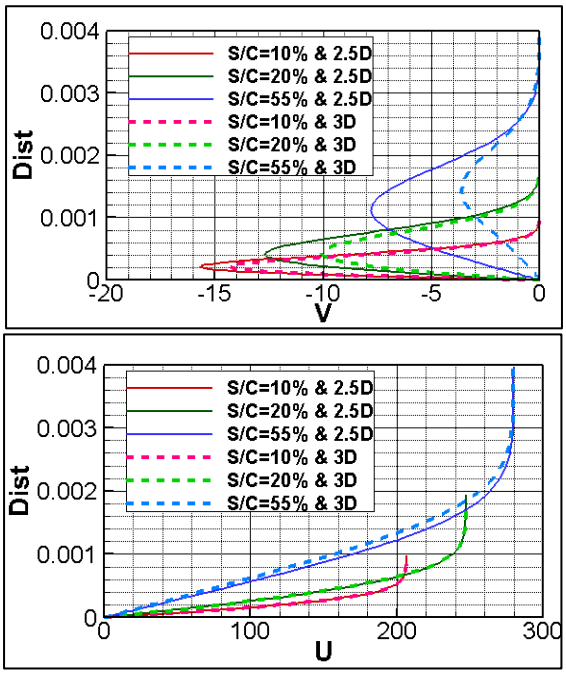


Figure 5: LSBJ test case. Section Y=5%. Comparison between 2.5D and 3D velocity profiles for 3 stations. (S/C=0.1, 0.2 and 0.55). Upper part: transverse velocity component. Lower part: longitudinal velocity profiles.

5.2. Interpolation strategy

Transition line interpolation strategy also needs to be clarified. When the transition line evolves smoothly over the spanwise direction, linear interpolation from a limited number of spanwise sections (Fig.6, upper side transition line for the LSBJ case made of 5 spanwise sections, blue line) is sufficient.
Nonetheless, a pattern change in the transition mechanism may lead to an interpolation error. For example Fig.6 lower part, transition is triggered by CF instabilities for Y<0.3 then TS instabilities (Y>0.3). The discontinuity exhibited around Y=0.3, shows that interpolation error greatly depends on the number of sections and their locations. Therefore two options are available:
The first possibility is an algorithm that detects the shift in transition instabilities and decides where to add cuts or not, in order to minimize the

interpolation error.
The second possibility is to increase the number of sections. It is possible to take into account a sufficiently large number of sections in order to cover the entire wing with structured meshes.

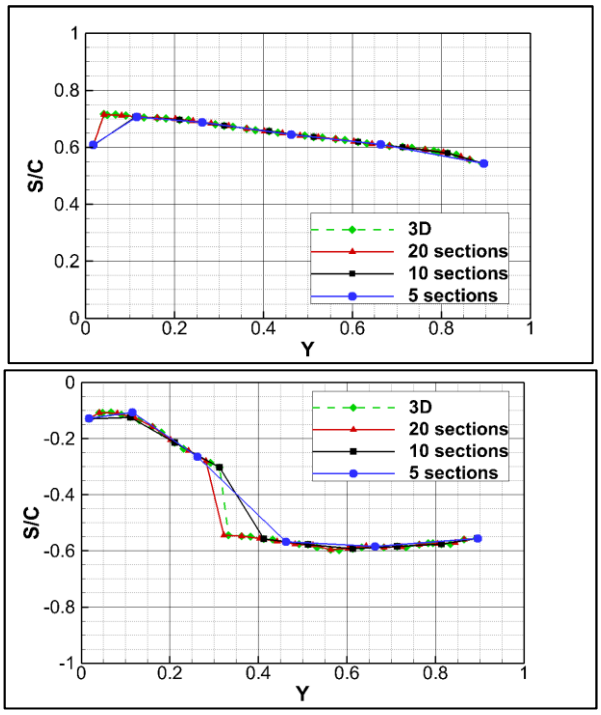


Figure 6: LSBJ test case, comparison of transition line interpolation with 5, 10 and 20 sections for an intermediary solution. e^N transition criterion. Upper part: suction side; Lower part: pressure side.

5.3. Validation: comparison between Aether coupled with 3c3d and elsA (ONERA)

Fig.7 displays results obtained by ONERA and Dassault Aviation. ONERA uses the C1 & AHD criteria implemented in elsA. The dark blue color represents the laminar flow and the light blue color the turbulent flow.
Dassault Aviation obtained two transition lines (based on 10 spanwise transition positions) using the transition chain, the yellow line corresponds to the C1 and AHD criteria and the red line to the e^N method.
First, the difference encountered at the suction side is due to the coupling process. As said in §4.5 when transition is predicted near the sonic shock, its position is intentionally locked during the process. Due to C1 criteria early triggering, the transition line is skewed. This could be arranged by using an intermittency function, but the choice was made in order to avoid buffeting. The process of locking the transition position near the shock may be reconsidered if the wind tunnel data show too much discrepancy. However, this strategy has demonstrated to be sufficiently accurate and robust until now.
Second, the good match between both processes (from ONERA and from Dassault Aviation) using the C1 & AHD criteria for the pressure side validates our transition chain.
Third, differences between e^N method and C1 & AHD criteria are observed. There are three regions at the pressure side:

- A first area (Y<0.4, region 1), where CF initiated the transition for both criteria.
- A second area (Y= [0.4; 0.7], region 2), where C1 criterion predicted transition, although the e^N method detected a TS transition.
- Finally, a third area (Y>0.7, region 3), denoted by a correct agreement between the 2 prediction criteria attributed to TS predicted transition.

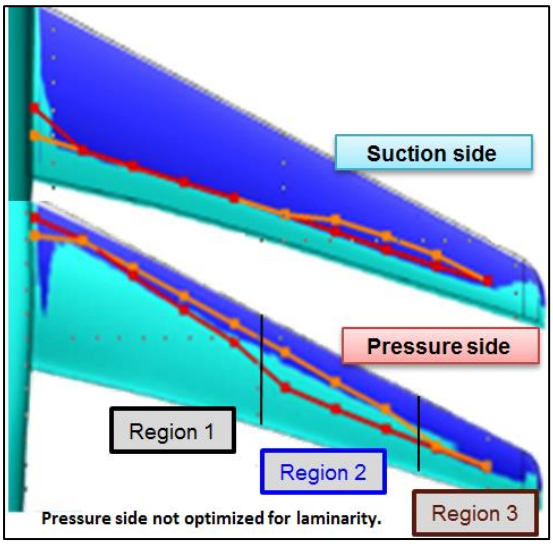


Figure 7: LSBJ test case. Comparison between Dassault Aviation and ONERA transition lines.
Dassault Aviation: C1 & AHD transition line in yellow. e^N method in red. ONERA (Elsa): C1 & AHD criteria. Laminar flow (respectively turbulent) is plotted in dark blue (respectively light blue). ***The wing will include a Kruger on pressure side.***

In the first region, this difference can be allocated to C1 criterion which may be conservative. C1 criterion is made from wind tunnel database where conditions are rougher than the flight conditions. The match between $N_{CF_{limit}} = 0.85 * N_{CF_{Trans}}$ (green line) and C1 criterion (yellow line) for Y<0.3 (as represented in Fig.8) is a proof whereas transition prediction with $N_{CF_{limit}} = N_{CF_{Trans}}$ has been accurate for the Falcon 7X horizontal tail plane (see §6.1).
For the second region, the reduction of $N_{CF_{limit}}$ from $N_{CF_{Trans}}$ to $0.85 * N_{CF_{Trans}}$ was not possible to correct the difference in prediction between both methods ($N_{CF_{limit}} = 0.85 * N_{CF_{Trans}}$, green line and C1 criterion, yellow line), neither a diminishing of

$\Psi_{(CF|TS)}$ value to 40° (pink line). Generally $\Psi_{(CF|TS)}$ = 60° gives a good estimation of the switch between CF and TS instabilities domination for subsonic and transonic flow, but in reality it can progress more smoothly and make the determination of $\Psi_{(CF|TS)}$ harder to use. Therefore, the diminished value of $\Psi_{(CF|TS)}$ can be seen like an expansion of the CF zone in order to reach a higher value of the N factor and brought on CF induced transition.

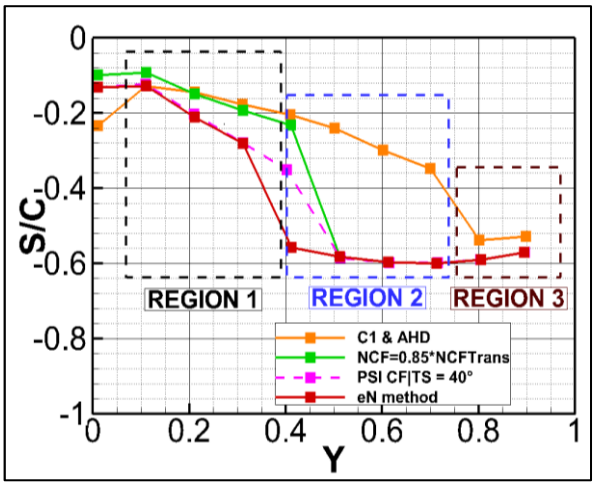


Figure 8: LSBJ test case. Transition line comparison. Wing pressure side (Lower side).

Finally, a reduction of 30% of $N_{CF_{limit}}$ ($N_{CF_{limit}}$ =0.70*$N_{CF_{Trans}}$) (not plotted) showed a better agreement for this region but was excessively conservative for the first region. The discrepancies between C1 criterion and e^N may be clarified once wind tunnel data will be available.

6. CROSS FLOW INDUCED TRANSITION

For some time C1 and AHD were at the forefront, but during the last decade, the e^Nmethod gained popularity. Results obtained from the Dassault Aviation transition chain for C1 & AHD and the e^N method are presented and discussed here.

6.1. Horizontal Tail Plane Falcon 7X

The emphasis is aimed at CF induced transitions using recent flight test campaigns performed in the framework of CLEAN SKY/SFWA in December 2010 and April 2012. Due to the camera location positioned on the vertical fin, results for the upper side of the horizontal tail plane (HTP) only were available. The cruise speed corresponds to a Mach number of 0.75. In order to have an exploitable laminar region, the HTP is deflected to a 4° angle of attack during the flight. Numerical computation done with the transition chain displayed $\bar{R} < 250$ over the HTP span. The contamination criterion was not triggered and authorized the study of laminar transition.

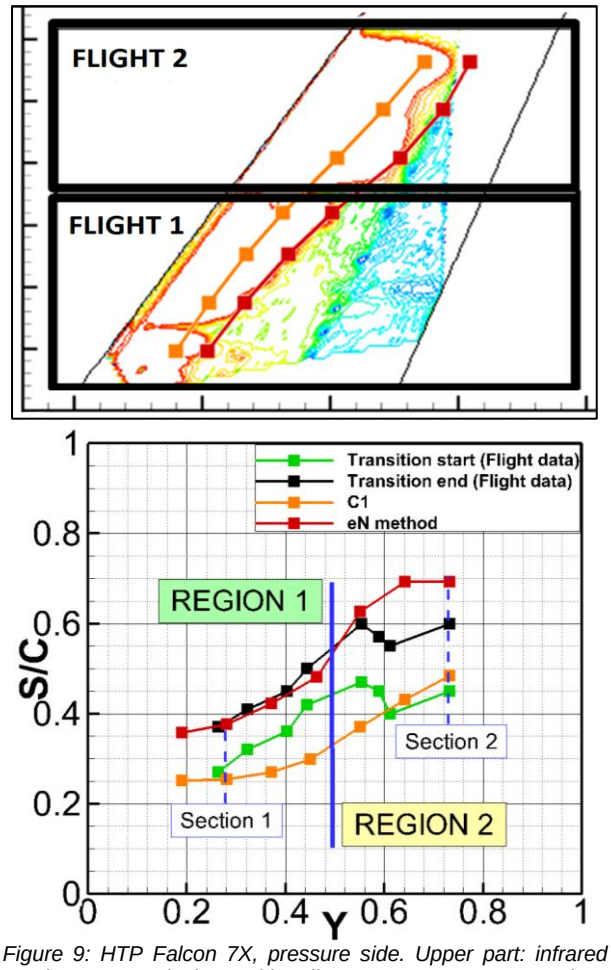


Figure 9: HTP Falcon 7X, pressure side. Upper part: infrared results & numerical transition lines. Lower part: comparison between numerical and experimental transition lines.

Fig.9 lower part, displays the lines corresponding to the end of transition (respectively the line corresponding to the beginning of transition) detected by IR analysis in black (respectively in green). The transition line for the C1 & AHD criteria is displayed in yellow while the e^Nmethod transition line is in red.

Comparisons between the C1 & AHD criteria (yellow line) and flight data (black line) show that the semi-empirical criteria trigger the transition too early with respect to the flight data. In fact, the transition is detected too early by the C1 criterion. As previously mentioned in §4.3.3 C1 criterion is a local criterion which does not take into account stability history of the BL. Nevertheless, it still manages to predict the beginning of transition with an error of less than 10% of chord.

Comparisons between e^N (red line) and flight data (black line) show two regions:

Region 1, Y<0.5: CF vortices are responsible for triggering the transition. The e^N method criterion is really efficient, the difference between numerical and flight data (end of transition black line) is less

than 5% of chord.
Transition analysis and exact stability results are plotted for section Y=0.28 in Fig.10. A short zone (S/C = [0.10; 0.15]) of Ψ <60° is perceptible for the parabola method. As said in §4.3.5, a smoothing algorithm is applied in order to suppress erratic behavior due to database interpolation and to distinguish CF clearly from the TS zone.

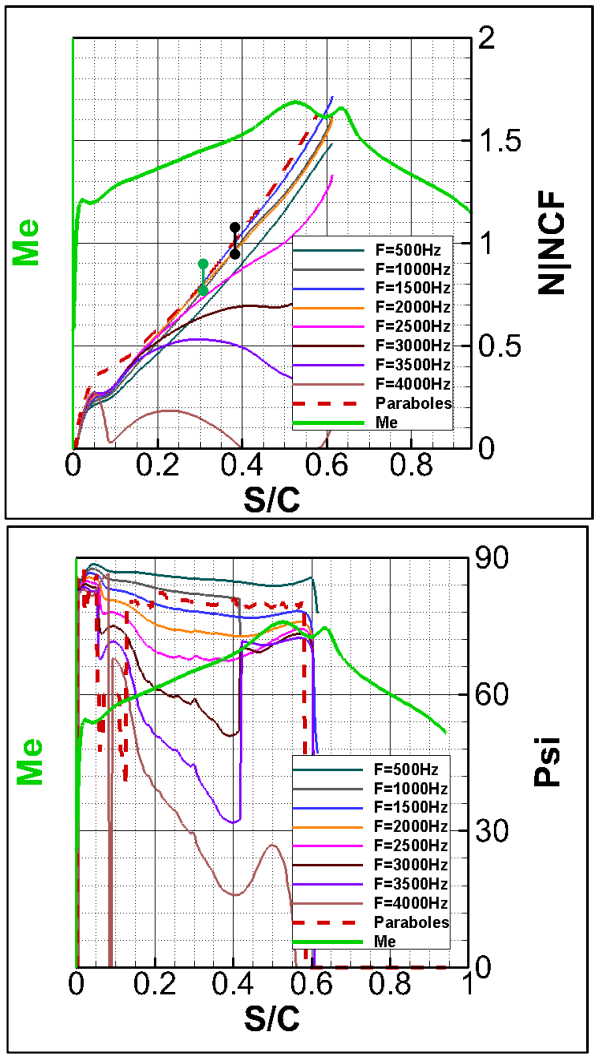


Figure 10: comparison between exact stability analysis (code CASTET) and parabola method (red line). Y=0.28 pressure side. Upper side: N factor. N|NCF=$N/N_{CF_{Trans}}$. Lower side: Ψ parameter. First sign of transition is symbolized by ⏐● *and the end of transition by* ●⏐.

The exact stability analysis performed with CASTET justifies the smoothing practice. The most unstable disturbances have frequencies between 1000 to 2000 Hz.
For S/C= [0.10; 0.15], 2000 Hz frequency (the orange line) is the most unstable and has a Ψ >60°.
Globally, the parabola method approximates the N factor and the Ψ parameter well, except for the small zone S/C = [0.05; 0.15] due to the kink in local Mach number near S/C=0.05. However, the overestimation of the N factor is not relevant and positions of transition detected by both methods (the parabola method and the exact stability method) for Ψ>60° (CF) are practically at the same location $S/C_{\ Trans} = S/C_{(N|NCF=1)} \approx 0.4$.
Region 2, Y>0.5, a succession of CF/TS/CF dominated patterns are identified. This complex sequence of patterns is not well represented by the transition criterion. Succession of patterns is due to a small deceleration getting amplified over the external part of the HTP (Fig.11, right upper corner) and being accompanied by a decrease of pressure gradient for S/C = [0.2; 0.6] (Fig.11, left upper corner) which results in a stabilization of the disturbances (Fig.11, left bottom corner) and multiple CF/TS zones (Fig. 11 right bottom corner).

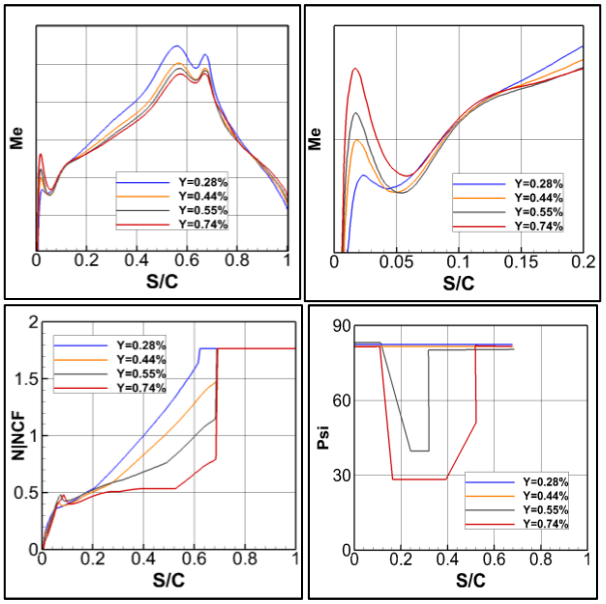


Figure 11: Evolution of the Mach number, N factor (parabola method) and Ψ parameter (parabola method) for 4 spanwise slices (pressure side). N|NCF=$N/N_{CF_{Trans}}$.

In order to clarify differences between transition data (infrared results) and the e^N method, an analysis for Y=0.7 is presented in Fig. 12. Comparison between the Parabola method and the exact stability analysis shows interesting results. Three patterns are identified in both analyses. The exact stability analysis shows:

- A first zone S/C = [0; 0.15]. The most amplified instability has a frequency of 4000 Hz with ψ>60° (CF vortices dominated in the BL). For the exact stability analysis N factors have a maximum value of $\approx 0.15 * N_{CF_{Trans}}$ while for the Parabola method N factor grows from 0 to $\approx 0.6 * N_{CF_{Trans}}$. It also contains the

decelerated flow visualized also in Fig. 11, in the right upper corner (red line).

- A second zone S/C= [0.15; 0.3]. The most amplified instabilities have frequencies from 4000 Hz down to 2000 Hz with ψ = [30°; 40°] (TS dominated).
- A third zone S/C= [0.3; 0.7]. The most amplified instabilities have frequencies between 1500 and 2000 Hz and consisted in CF (ψ>60°).

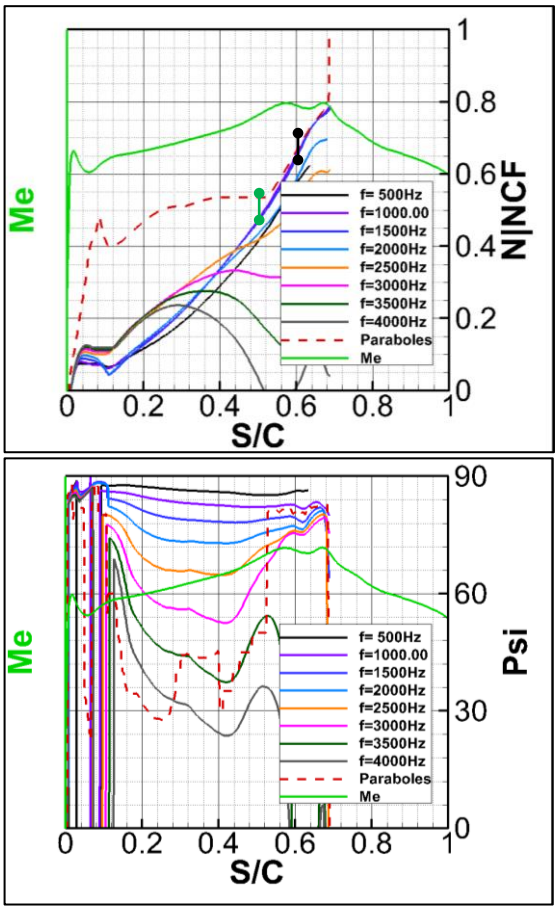


Figure 12: Parabola and exact stability analysis. HTP Falcon 7X. Y=0.74, pressure side. N|NCF=$N/N_{CF_{Trans}}$. The first sign of transition is symbolized by and the end of transition by .

The deceleration stabilized CF instabilities which explains the small value of the N in the first region, but also amplified TS instabilities. The TS zone corresponds to the effect of the decelerated flow, and the weak pressure gradient between S/C = [0.1; 0.5] tends to emphasize this phenomenon. It maintains the growing up to S/C=0.3 of instabilities which are the most amplified for low values of Ψ directions and are characterized by frequencies higher than 2000 Hz.

The presence of the near leading edge decelerated flow which grows spanwise could be the consequence of an aero-distortion of the HTP; this hypothesis is discussed in §6.2 below. As a matter of fact, the sequence CF/TS/CF is not common, and very limited data sets are available. This also explains the overestimation of the N factor provided by the parabola method. The parabola method is for the moment not well adapted to such complex flows which present patterns of "sawtooth" flow (accelerated, decelerated…). One must keep in mind that it is an approximation method, fast and efficient for "almost" all configurations, and as Fig.12 displays, further downstream the decelerated flow, (S/C = [0.5; 0.7]) the two methods (parabola and exact stability analysis) are again in perfect match.

There is still one last thing to verify and that could explain the shift in transition for region 2: it is possible that the shape used for doing the calculation is not exactly representative of the Falcon 7X due to aero-distortion. The HTP was deflected to an angle of attack of 4° during the flight in order to ensure laminar flow. Normally, at cruise speed, a smaller angle of attack is used.

6.2. Aero distortion

The estimation of deformation due to aero-distortion showed two things:

- Pressure and suction sides being inverted on the HTP, the depression is accentuated and generates an increase in flexion of ≈-60 mm (Fig. 13, left side) between the root of the wing and the end.
- The deflected angle of attack generates a slight twist of the HTP described by Fig. 13, right side.

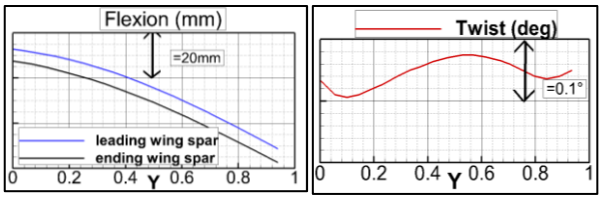


Figure 13: flexion (left side) and twist (right side) corresponding to the aero distorted flight test HTP Falcon 7X with an incidence angle of 4°.

Flexion and twist are both taken into account by an in house Dassault Aviation deformation tool. This tool generates a new shape, more faithful to the HTP Falcon 7X used for flight test with the deflected angle of attack of 4°.

A comparison between the two shapes is presented in Fig. 14: in blue the original HTP, not distorted; in pink, the aero distorted shape. As far as one can see, distortions are located in zones where decelerated flow was detected (near the leading edge). New RANS computations using the transition chain were performed for both transition criteria (C1 & AHD and e^N method).

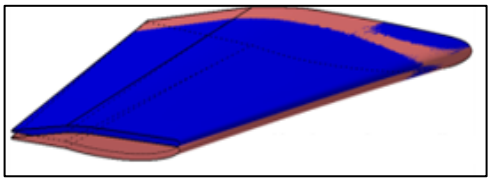


Figure 14: superposition of both reference and deformed shapes. Blue, original shape. Pink, distorted shape.

Juxtaposition of transition lines (Fig. 15) between the two shapes indicates slight effects of aero distortion on the transition mechanism. Aero distortion was neither responsible for generating the deceleration near the leading edge nor conducting a smaller value of N factor.

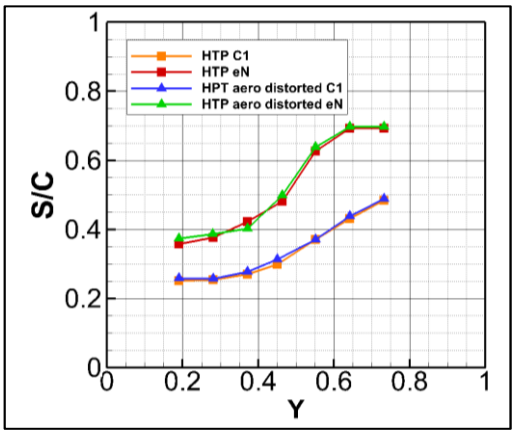


Figure 15: transition lines comparison for distorted and non-distorted shape.

6. CONCLUSIONS

The development and validation work performed to achieve accurate and efficient prediction of transition has been described.

A number of challenges from transition models will require further research and development efforts. This includes the modeling of the well-known transition in a laminar separation bubble, in particular the long bubble that can appear when a laminar boundary layer interacts with a shock wave.

Another issue recently observed is associated to a complex transition phenomena observed when sequences of successive CF and TS behaviors are present along a given streamline.

One possible source of remaining differences between parabola method results and flight data could have been the impact of aerodynamic distortion on the pressure coefficient calculation. However, this was ruled out by further calculations on a distorted geometry. This therefore confirms that the discrepancy is to be directly linked to the difficulty of the current transition criterion to properly account for multiple CF/TS/CF sequences.

REFERENCES

[1] M. Arthur and C. Atkins, "Transition modelling for viscous flow prediction," in *38th AIAA Fluid Dynamics Conference and Exhibit*, San Francisco, California, 2006.

[2] A. Krumbein, N. Krimmelbein and G. Schrauf, "Application of a Hybrid Navier-Stokes Solver with Automatic Transition Prediction," in *25th AIAA Applied Aerodynamics Conference*, Miami, Florida, 2007.

[3] F. Chalot, M. Mallet and M. Ravachol, "A comprehensive finite element Navier-Stokes solver for low- and high-speed aircraft design," in *AIAA 32nd Aerospace Sciences Meeting*, Reno, Nevada, 1994.

[4] J. Perraud, O. Vermeersch and R. Houdeville, "Decriptif et mode d'emploi du code 3C3D V5.4.8," Toulouse, 2011.

[5] W. Pfenninger, "Laminar flow control - Laminarization," AGARD, Rhode-St.-Genese, Belgium, 1977.

[6] G. B. Schubauer and H. Skramstad, "Laminar-boundary-layer oscillations and transition on a flat plate," N.A.C.A., Washington D. C., 1943.

[7] W. Saric, "Experiments in 3-D Boundary Layers: Stability and Receptivity," in *RTO-EN-AVT-151 - Advances in Laminar-Turbulent Transition Modelling*, Rhode St. Genèse, Belgium, 2008.

[8] D. Arnal, G. Casalis and R. Houdeville, "Practical Transition Prediction Methods: subsonic and transonic flows," NATO, 2008.

[9] W. S. Saric, "Introduction to Linear Stability," NATO, 2008.

[10] J. Perraud, "Stabilité locale linéaire des couches limites 3D compressibles. Mode d'emploi et description du code CASTET," Toulouse, 2009.

[11] J. Perraud, D. Arnal, G. Casalis, J.-P. Archambaud and R. Donelli, "Automatic Transition Predictions Using Simplified Methods," *AIAA Journal,* vol. 47, pp. 2676-2684, November 2009.

[12] L. M. Mack, "Transition Prediction and Linear Stability Theory," in *AGARD Conference Proceedings*, Paris, FRANCE, 1977.

[13] D. Arnal, E. Coustols and J. Juillen, "Etude expérimentale et théorique de la transition sur une aile en flèche infinie," *La Recherche Aérospatiale,* 1984.